NeuroReport 10, 2911–2917 (1999)

Mapping biochemistry to metabolism: FDG-PET and amyloid burden in Alzheimer's disease

Michael S. Mega,[1,2,CA] Teresa Chu,[2,3] John C. Mazziotta,[1] Kashyap H. Trivedi,[1] Paul M. Thompson,[1] Amish Shah,[1] Gregory Cole,[2] Sally A. Frautschy,[2] and Arthur W. Toga[1]

[1]Department of Neurology, Laboratory of Neuro Imaging, Division of Brain Mapping, [2]Alzheimer's Disease Center, and [3]Department of Medicine UCLA School of Medicine, 710 Westwood Plaza, Rm 4-238 Reed, Los Angeles, CA 90095-1769, USA

[CA,1]Corresponding Author and Address

We evaluated the relationship between amyloid-β protein (Aβ) concentration and the metabolic abnormality in an Alzheimer's disease (AD) patient as measured by [^{18}F]fluorodeoxyglucose positron emission tomography (FDG-PET). Across most regions there were significant inverse correlations among FDG-PET intensity values and both insoluble. The temporal lobe samples showed no significant correlation between FDG-PET values and Aβ deposition. Findings support Aβ as contributing to the hypometabolism in regions of the AD brain that are still relatively viable metabolically; those regions with chronic pathologic damage, such as temporal cortex, may have other factors that contribute to metabolic deficits. *NeuroReport* 10:2911–2917 © 1999 Lippincott Williams & Wilkins.

Keywords: Alzheimer's disease; Amyloid protein; Brain mapping; PET

Introduction

The relationship between the metabolic defect in Alzheimer's disease (AD), as measured by [^{18}F]fluorodeoxyglucose positron emission tomography (FDG-PET), and the cellular markers of the disease is poorly understood. Atrophy is the best correlate to focal hypometabolism [1,2]. In a pathological study conducted 16 months after an AD patient was evaluated with FDG-PET, regional hypometabolism correlated with cell loss, gliosis and amyloid plaques [3]. In that study the PET was obtained long before the post-mortem evaluation and tissue samples were not precisely localized to the PET data.

Amyloid is deposited in the posterior parietal lobe early in AD [4]. Medial temporal structures are affected early in mildly impaired patients [5] but are not well visualized by PET. The preclinical parietal hypometabolism supports a role for amyloid in the pathophysiology of AD. Although amyloid containing plaques do not correlate with cognitive deficits in AD [6] or disease duration, altered synaptic function is associated with the accumulation of amyloid β-protein (Aβ) [7]. The activity observed on FDG-PET, assuming that blood flow and glucose utilization remain coupled, reflects the metabolism of active synapses as they restore their resting ionic gradients via Na/K-ATPase [8]. Metabolism of glucose and the production of ATP from the electron transport chain in mitochondria concentrated in synapses may be dysfunctional in AD due to oxidative damage [9].

Oxidative damage is increased in AD compared with age-matched controls, as reflected by increased mitochondrial DNA deletions [9] due to the generation of reactive oxygen species (ROS), increased lipid peroxidation [10] and an increase in the cell's attempt to generate reducing power by up-regulating glucose-6-phosphate dehydrogenase [11]. If Aβ causes oxidative damage *in vivo*, then disordered energy metabolism reflected by low FDG-PET values should be significantly associated with high levels of Aβ. This study tests the above hypothesis by measuring Aβ concentrations in fresh frozen brain samples mapped to their spatial location in the same patient's pre-mortem functional imaging data. By employing both linear and non-linear [12] warp-

ing algorithms cryomacrotome tissue deformations are corrected allowing metabolic–biochemical analysis.

Materials and Methods

Patient: The patient was a right-handed man, employed as a circuit court judge, who died at the age of 80 years with a premorbid diagnosis of probable AD as defined by the National Institute of Neurological and Communicative Disorders and Stroke/Alzheimer's Disease and Related Disorders Association [13]. Symptoms first appeared approximately 10 years prior to death manifested by apathy and forgetfulness. Instrumental activities of daily living (paying bills, writing checks, shopping, etc.) were lost 5 years prior to death. Activities of daily living (feeding, bathing, toileting, etc.) were lost 3 years prior death. A gradual decline of other functions ensued with no evidence of systemic, metabolic or focal brain abnormalities revealed by laboratory analysis and structural imaging. A FDG-PET study was obtained 8 h before death and the patient's brain was frozen 12 h after death. At the time of scanning the patient's neurological examination was significant for eyes open with blinking to threat bilaterally. The patient had no spontaneous verbal output and did not follow commands. With painful stimuli the patient moved all extremities equally; there was no asymmetries on deep tendon reflexes and toes were down-going. The cause of death was cardiopulmonary arrest. The patient had a neurofibrillary tangle burden, as reflected by Gallyas staining intensity, consistent with Braak and Braak stage IV [14], as reported previously in a methodological description [15]. This study was approved by the Human Subjects Protection Committee of the University of California at Los Angeles, and the patient's nearest relative signed a written informed consent.

Scanning procedure: Arrangements were made to scan the patient with FDG-PET when death appeared imminent, and the patient's family signed an informed consent for scanning. During uptake the room was dimmed, the patient received a 5 mCi i.v. injection of [^{18}F]fluorodeoxyglucose (half life 110 min) according to a protocol described previously [16]. Scanning was performed on a Siemens ECAT 961 scanner that produces 47 slices. Images were reconstructed with a Hanning filter for a final image resolution of 3.6 mm FWHM inplane at center and 4.5 mm at 20 cm off-center. A calculated attenuation correction was used [17]. The FDG-PET voxel is 1.69 mm in the x and y dimensions and 3.125 mm in the z axis. Imaging commenced 40 min after administration of FDG and lasted for 60 min, with >2 million counts per plane. We did not obtain absolute metabolic rates in this study; all functional images reflect FDG-PET intensity values referenced to a peak in the patient's cerebellum. The patient's head was immobilized using a polystyrene head-holder. Continuous pulse-oximeter readings of the patient during scanning never fell below 92% saturation.

Tissue collection: Cryomacrotome sectioning of the frozen tissue produced whole brain sections for tissue samples and allowed the reconstruction of a 3D digital data set. Within 6 h of death, the brain was prepared by *en bloc* frozen fixation starting at a temperature of 10°C and then lowered into a isopentane bath at −70°C at a rate of 1 cm/min. The frozen brain was then sectioned in the coronal plane in a large industrial cryomacrotome (PMV Stockholm, Sweden) using a hardened steel knife. Image capture was accomplished by a Dage-MTI digital camera integral to the hydraulic descending blade allowing in-register capture of serial blockface images throughout sectioning. Digital images were captured every 500 μm; every 2 cm a 500 μm whole brain slice was obtained and cut by a 1.5 cm^2 grid die cutter as shown in Fig. 1. Once a digital image of this grid cut slice was obtained for later warping (thawing occurred for ∼1 min) it was stored at −70°C for later biochemical analysis.

Image processing Sectioning of the block face, with digital capture after each 500 μm cut, resulted in 320 images of high resolution ($1472 \times 1152 \times 320$; with 114 μm^2 pixels). This digital volume was then reduced to a 10.2 Mbyte file ($368 \times 288 \times 159$; one pixel = 457 μm^2 and z = 1 mm). The background and nonbrain tissue were digitally removed from this dataset and a surface model was constructed. Given the minimal anatomic deformation resulting from cryo-preparation, the premortem FDG-PET was then coregistered to the digital cryo dataset using a six parameter rigid body algorithm rather than a multiparameter transformation. A surface model of the patient's brain derived from the reconstructed cryosectioned dataset with the coregistered FDG-PET is shown in Fig. 1. Any slice in this model can be viewed on a computer screen and serves as a spatial reference for both the premortem PET and the fresh frozen tissue slices.

Digital images of the tissue sections acquired for biochemical analysis were then registered to the reference cryo-space using a 3D elastic warping algorithm described previously [12,15]. Briefly, target and reference contours drive the warp to correct tissue deformation. The algorithm treats tissue as an elastic material and pulls the anchored contours,

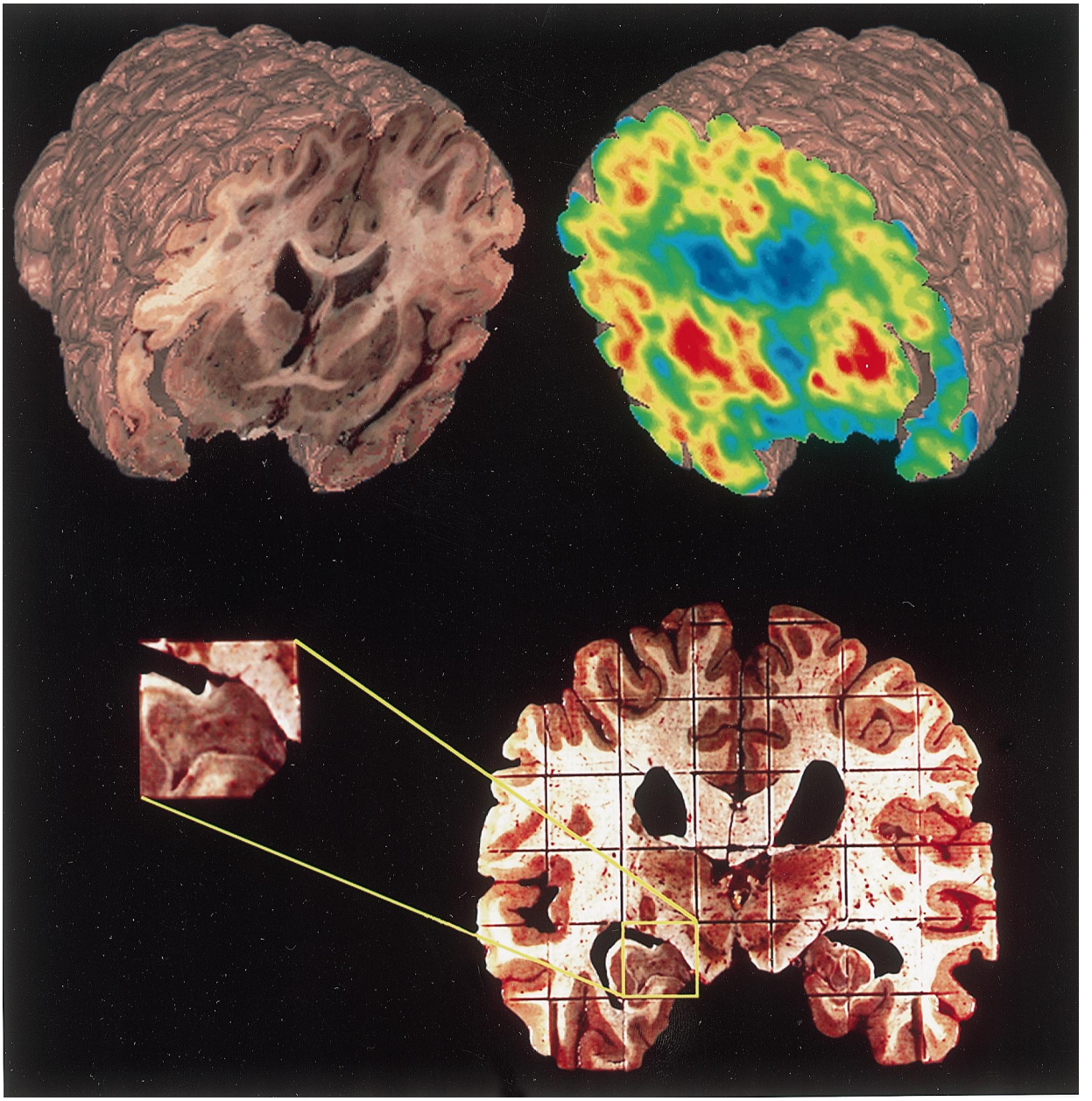

FIG. 1. Biochemical analysis was accomplished with the cryomacrotome harvested snap frozen tissue. Using a grid die cutter 1.5 cm^2 samples were obtained and stored for future analysis. The location of each grid sample within the slice is referenced to this digital image that will subsequently be elastically warped back into the cryo-space that allows 3D reconstruction and PET registration.

interactively drawn on the sections, into register with the corresponding target contours of the cryo image. The elastic warp was performed on grid slices obtained every 2 cm from the anterior to posterior limit of the brain in the coronal plane. The result of these deformation corrections applied to a fresh frozen section is shown in Fig. 2. Registration of the PET data with the cryo structural volume was accomplished with a six parameter rigid body alignment [18] to minimize PET voxel distortion. Excellent registration can be achieved for the purpose of PET comparisons using this approach even when the harvesting process distorts the tissue from its original morphology (Fig. 2b,c).

The mean FDG-PET values produced by each grid sample was determined by drawing regions of interest (ROIs) on the elastically warped grid image and then transferring them onto the PET image resampled in cryo-space (Fig. 2d). The CSF and white matter (WM) space was excluded from these ROIs by drawing outlines around only grey matter (GM) on the warped grids. From the high resolution cryomacrotome image the quantity of GM pixels (with a known dimension of 0.457×0.457 mm) was

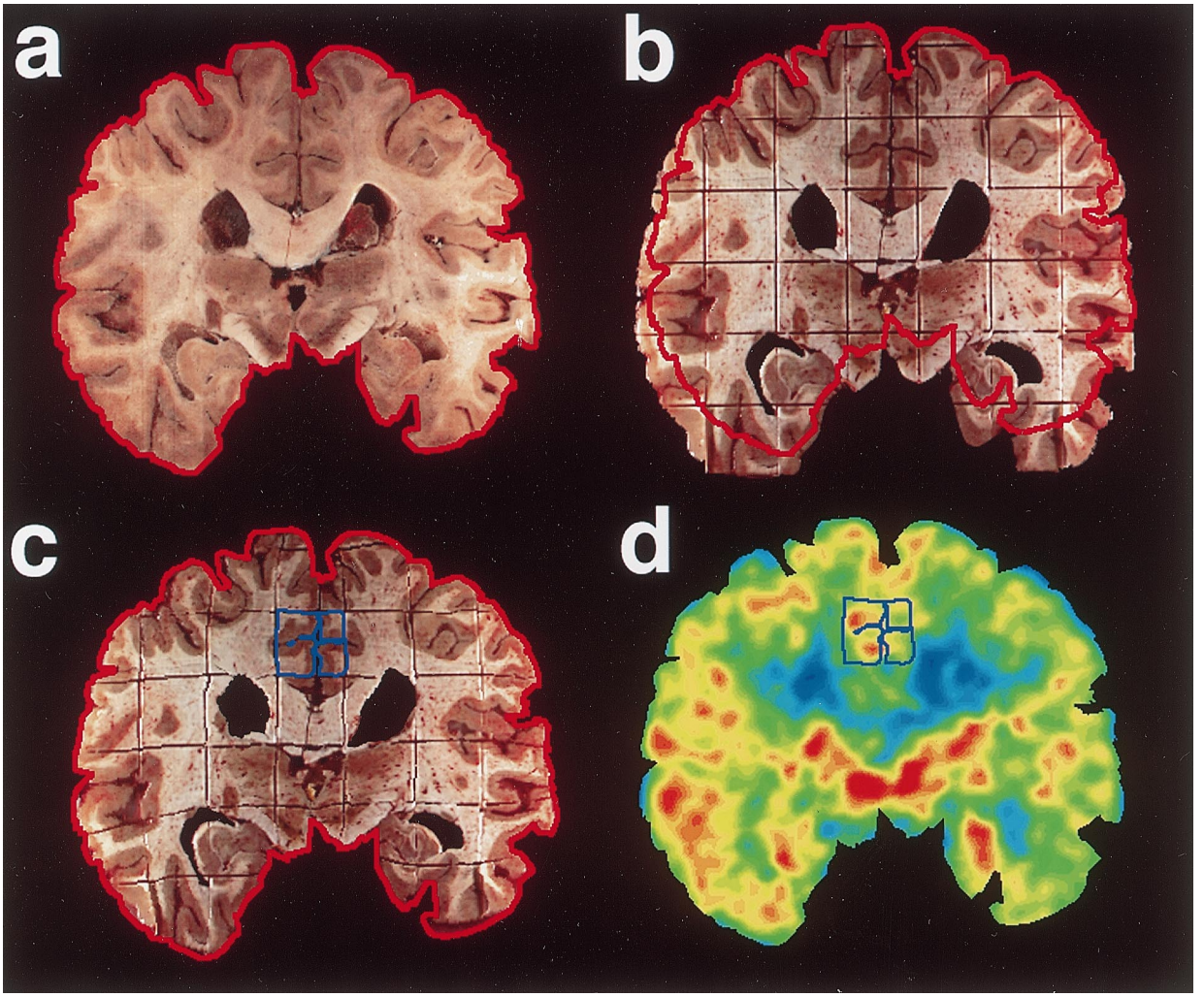

FIG. 2. The cryo-space is derived from a digital image of the tissue (**a**) prior to harvesting from the whole brain block-face. The target outline is shown in red. The fresh frozen tissue section (**b**) is elastically warped back into the cryo-space using a modified 3D warping algorithm (**c**) [12]. Concentrations of amyloid β-protein (Aβ) can be assayed from aliquots of the grid samples, outlined in blue (white matter and csf pixels are excluded in analysis), using a sandwich ELISA with antibodies specific to Aβ and compared to the mean FDG-PET intensity values referenced to a peak in the cerebellum (d) and co-registered to the cryo-space.

calculated for each tissue sample. This GM pixel quantity was used to derive the volume of GM (mm^3) in each 500μm thick tissue sample producing the metabolic data. By referencing the metabolic and biochemical data to the volume of GM in each tissue sample sufficient correction of the partial volume imaging error and differing GM proportions of the tissue samples can be achieved.

Biochemical analysis: Cellular Aβ was quantitated from 66 grid locations, of varying metabolic values, with a sandwich enzyme-linked immunoabsorbent assays (ELISA) [19] utilizing two Aβ peptide specific antibodies. Mouse monoclonal 4G8 against Aβ aa 17-24 (Senetek, Maryland Heights, MO) was used as the capture antibody, loaded at a concentration of 3 μg/ml in 0.1 M carbonate buffer, pH 9.6 onto a 96-well plate (Nunc Maxisorp). Blocking was completed with 2% bovine serum albumin (BSA) in Tris-buffered saline (TBS). Centrifugation of these samples at 100 000 × *g* at 4°C occurred for 20 min. Aβ in the pellet (insoluble fraction), separated from the supernatant (soluble fraction), was extracted with 70% formic acid. The suspended insoluble fraction was then centrifuged at 100 000 × *g* at 4°C for 45 min to separate the lipid content. Processed and neutralized samples were diluted with EC buffer (20 mM Tris, 400 mM NaCl, 2 mM EDTA, pH 7.4 with 1% BSA and 0.05% CHAPS) containing protease inhibitors (20 μg/ml each of pepstatin, aprotinin, leupeptin and phosphoramidon, 0.5 mM PMSF, 1 mM EGTA) and loaded into the wells. The detector antibody was biotinylated mouse monoclonal 10G4 against Aβ amino acids 5–13 [20], added at a final dilution of 1:1500 in TBS containing 1% BSA. The reporter system was streptavidin–alkaline

phosphatase (Vector Labs, Burlingame, CA) using AttoPhos (JBL, St. Luis Obispo, CA) as the substrate. Fluorescence of the AttoPhos product was monitored at an excitation wavelength of 450 nm and an emission wavelength of 580 nm with a CytoFluor II plate reader (PerSeptive Biosystems, Bedford, MA). A standard curve over a range of 0.02 to 10 ng was prepared from Aβ peptide and subjected to four-parameter fit by non-linear regression. Data (total Aβ 1-40 and 1-42 from samples) were analyzed by fitting to the equation derived from the standard curve. Since all grid aliquots had an equal volume, results are reported as ng of Aβ concentration in each sample referenced to the volume of GM in each grid.

Statistical analysis: Pearson correlations were computed for all FDG-PET intensity values (referenced to a peak in the cerebellum), with the Aβ levels. Because the PET and Aβ data did not generate a normal distribution, a bootstrap analysis [21] was employed to test the significance of the correlations. The program Resampling Stats was used to evaluate significance. Briefly, bootstrap analysis randomly mixes one of the dataset pairs (e.g. the PET measures) and a new r value is calculated based upon this randomization of the dataset pairing. This possible r value is recorded and the above procedure is repeated 1000 times, producing a distribution of possible r values from the observed dataset. The observed r value can then be compared with the distribution of the possible r values between randomized PET and Aβ data. The probability of finding the observed correlation based upon the distribution of possible correlations generated from the same dataset by resampling is then recorded. This process was repeated 10 times for each of the correlations reported to arrive at an average probability value for each comparison. If the observed correlation is greater than 95% of the correlations expected from random resampling in the bootstrap method, the observed difference was judged to be statistically significant at the 0.05 level.

Results

A regional analysis of the mean FDG-PET intensity values (referenced to a peak in the cerebellum) and Aβ tissue concentrations for both the soluble and insoluble fractions is shown in Fig. 3. The highest PET values were in regions with the lowest Aβ levels (cerebellum, thalamus and putamen); as Aβ levels increased from subcortical to cortical regions mean PET values declined. Across the cortex regional mean PET values increased from the temporal lobes spreading anteriorly and posteriorly, with the highest regional anterior metabolic activity in the anterior cingulate, and posteriorly in the medial occipital lobe.

Total brain samples showed a significant inverse relationship among FDG-PET values and insoluble ($r = -0.59$, $p < 0.001$) and soluble ($r = -0.42$, $p = 0.001$) Aβ (ng/mm^3 GM), however regional analysis showed stronger correlations among FDG-PET values and insoluble Aβ (ng/mm^3 GM) across the parieto-occipital ($r = -0.71$, $p < 0.001$) and prefrontal ($r = -0.67$, $p < 0.001$) tissue samples. Soluble Aβ demonstrated a significant inverse correlation with FDG-PET values in the parieto-occipital ($r = -0.67$, $p < 0.001$) and prefrontal samples ($r = -0.41$, $p = 0.05$). The temporal lobe samples showed no significant correlation between FDG-PET values and Aβ deposition. Figure 4 shows the relationship between Aβ tissue fractions and the regional mean FDG-PET values for the entire dataset.

Discussion

This is the first study to map a biochemical marker of disease, using fresh frozen brain tissue, to its spatial location in the same patient's pre-mortem functional imaging data. Linear and nonlinear [12] warping algorithms corrected the spatial misalignments and tissue deformities to allow metabolic/biochemical analysis of human brain tissue. The initial application of this methodology in our patient has implicated Aβ as contributing to the metabolic abnormalities seen on FDG-PET in AD in prefrontal and parieto-occipital but not temporal regions. The present findings of a significant inverse relationship between prefrontal and parieto-occipital cortical FDG-PET values and Aβ concentration in a single patient should be interpreted cautiously, the proximity of PET prior to death (8 h) nonetheless provides a rare opportunity for some preliminary observations. The high prefrontal Aβ levels found in this advanced AD patient are consistent with a posterior to anterior progression of plaque formation in AD [4,14]. The similar significant inverse relationship between Aβ concentration and mean FDG-PET values in the parieto-occipital region also supports the role of Aβ in the pathophysiology of altered synaptic metabolism.

Neuritic plaques consist of neuritic processes with associated proteins including Aβ (in an insoluble form), apolipoprotein E, immune components, and other moieties. The aggregation of Aβ is probably a dynamic process initiated by the Aβ 1-42 amino acid sequence which precipitates the more soluble Aβ 1-40 protein [22]. Aβ is toxic to cultured neurons, increasing their vulnerability to metabolic insults

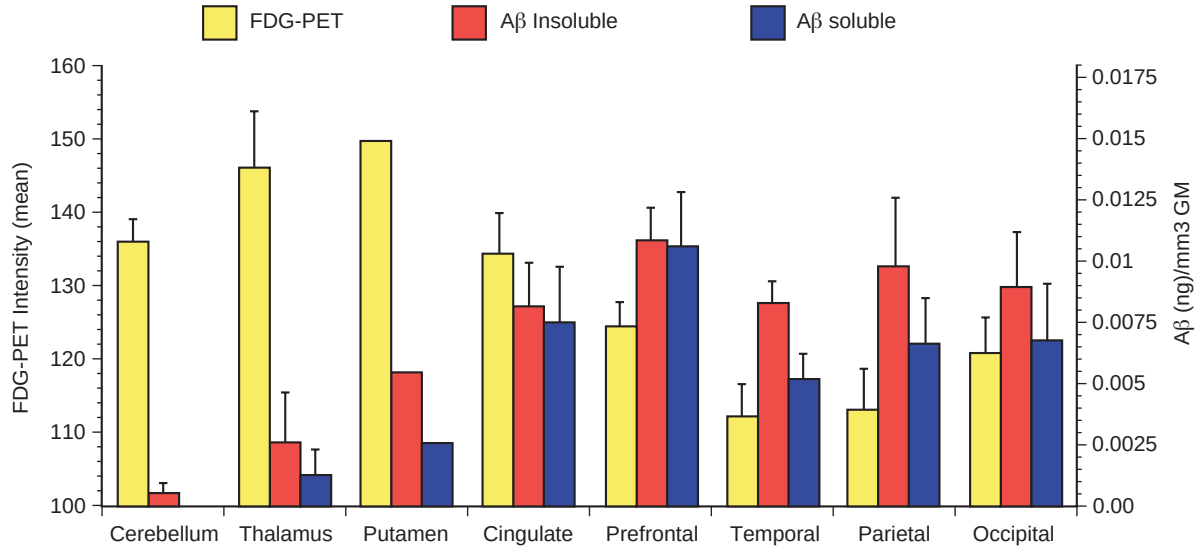

FIG. 3. Mean Aβ tissue concentration and regional FDG-PET intensity (referenced to a peak in the cerebellum) for all 66 samples, (error bars reflect s.e.m.). The putamen had a single sample from the left.

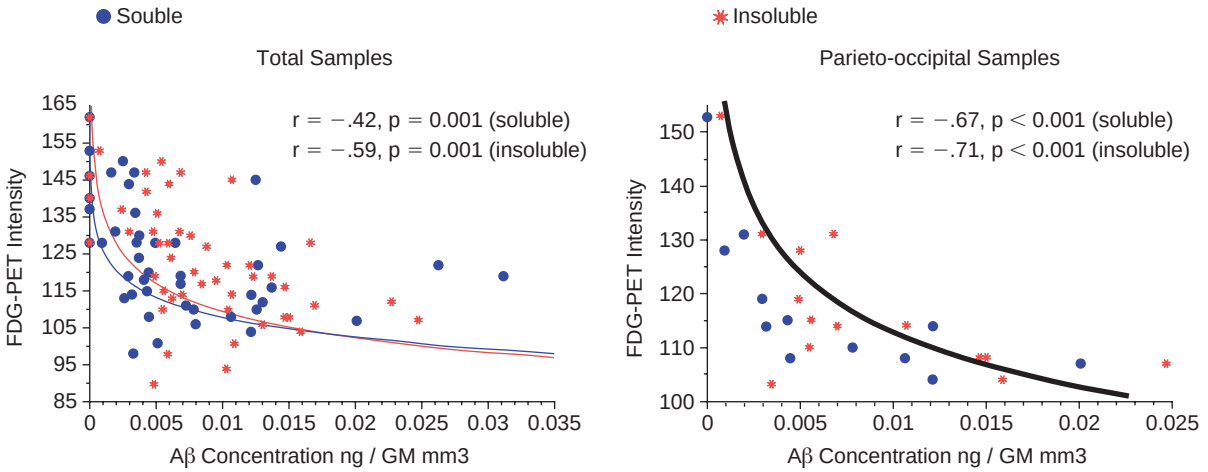

FIG. 4. Relationship between the soluble and insoluble Aβ tissue fractions (for all 66 samples) and FDG-PET intensity (referenced to a peak in the cerebellum) in the parieto-occipital region. Note the curves for the soluble and insoluble Aβ levels from the parieto-occipital samples are superimposed.

[23–26]. Damage may first effect the most metabolically active component of the neuron, the synapse. The poor inverse association in the temporal lobes bilaterally may implicate other disease mechanisms besides Aβ accumulation. Synaptic loss, diaschisis, or neurofibrillary tangles burden may better explain the metabolic defect in this region. If Aβ aggregation is a dynamic process then the lower average levels of Aβ in the temporal lobes may represent chronic changes and possibly clearance. Severe neuronal loss in the temporal region due to years of active disease may result in low levels of soluble Aβ production. Thus, the low mean FDG-PET values and low Aβ concentrations across most temporal regions may indicate that the acute disease process no longer affects this region and only the chronic effects of the disease are present in this patient. This lack of an association may reflect greater partial volume error in the temporal region not sufficiently corrected by our ROI method but this should also be the case in the prefrontal and parietal regions which also had severe cortical atrophy yet showed a robust correlation.

Future studies should map other markers across patients to enable a better understanding of the pathologic basis of the metabolic abnormalities in AD. Understanding the pathologic correlates of PET abnormalities in AD will also aid our interpretation of the functional imaging changes in aging and other disease processes.

References

1. Jamieson DG, Chawluk JB, Alavi A *et al. J Cerebr Blood Flow Metab* **7**, S410 (1987).
2. Fazekas F, Alavi A, Chawluk JB *et al. J Nucl Med* **30**, 1607–1615 (1989).
3. McGeer PL, Kamo H, Harrop R *et al. Neurology* **36**, 1569–1574 (1986).
4. Arnold SE, Hyman BT, Flory J *et al. Cerebr Cortex* **1**, 103–116 (1991).
5. de Santi S, de Leon MJ, Rusinek H *et al*. Selective medial temporal lobe pathology in cases at risk for Alzheimer's disease: diagnostic role of positron emission tomography. In: Iqbal K, Mortimer JA, Winblad B *et al.*, eds. *Research Advances in Alzheimer's Disease and Related Disorders.* New York: John Wiley, 1995: 173–180.
6. Terry RD, Masliah E, Salmon DP *et al. Ann Neurol* **30**, 572–580 (1991).
7. Terry RD, Maslaih E, Hansen LA. Structural basis of the cognitive alterations in Alzheimer disease. In: Terry RD, Katzman R and Bick KL, eds. *Alzheimer Disease.* New York: Raven Press, 1994: 179–196.
8. Kadekaro M, Crane AM and Sokoloff L. *Proc Natl Acad Sci USA* **82**, 6010–6013 (1985).
9. Mecocci P, MacGarvey U and Beal MF. *Ann Neurol* **36**, 747–751 (1994).
10. Palmer AM and Burns MA. *Brain Res* **645**, 338–342 (1994).
11. Balazs L and Leon M. *Neurochem Res* **19**, 1131–1137 (1994).
12. Thompson PM and Toga AW. *IEEE Trans Med Imaging* **15**, 1–16 (1996).
13. McKhann G, Drachman D, Folstein M *et al. Neurology* **34**, 939–944 (1984).
14. Braak H and Braak E. *Acta Neuropathol* **82**, 239–259 (1991).
15. Mega MS, Chen SS, Thompson PM *et al. Neuroimage* **5**, 147–153 (1997).
16. Barrio JR, MacDonald NS, Robinson GD *et al. J Nucl Med* **22**, 372–375 (1981).
17. Siegel S and Dahlbom M. *IEEE Trans Neurol Sci* **39**, 1117–1121 (1992).
18. Woods RP, Mazziotta JC and Cherry SR. *J Comput Assist Tomogr* **17**, 536–546 (1993).
19. Suzuki N, Cheung TT, Cai XD *et al. Science* **264**, 1336–1340 (1994).
20. Yang F, Mak K, Vinters HV *et al. NeuroReport* **5**, 2117–2120 (1994).
21. Efron B and Tibshirani R. *Science* **253**, 390–395 (1991).
22. Iwatsubo T, Mann DM, Odaka A *et al. Ann Neurol* **37**, 294-299 (1995).
23. Koh J-Y, Yang LL and Cotman CW. *Brain Res* **533**, 315–320 (1990).
24. Yankner BA, Duffy LK and Kirschner DA. *Science* **250**, 279–282 (1990).
25. Mattson MP, Cheng B, Davis D *et al. J Neurosci* **12**, 379–389 (1992).
26. Mark RJ, Hensley K, Butterfield A *et al. J Neurosci* **15**, 6239–6249 (1995).

ACKNOWLEDGEMENTS: Grant Support for this work was provided by an NIA award (K08AG100784) to M.S.M., Human Brain Project (NIMH/NIDA: P20MH/DA 52176), NSF (BIR9322434), NLM (LM/MH05639), and NCRR (RR05956) to A.W.T., and an Alzheimer's Disease Center grant (AG 10123). Special appreciation goes to the family of the patient for their kindness and accommodation.

Received 21 June 1999; accepted 30 July 1999